Electronic Supplementary Material (ESI) for Chemical Communications.
This journal is © The Royal Society of Chemistry 2024

Supplementary information

Construction of a redox pathway through a polyoxometalate and covalent organic framework for H_2O_2 photosynthesis

Yin Gong,[a,‡] Hongda Ren,[b,‡] Xiaojing Sang,[a]* Haotian Zhu,[a] Jingzhen Zhang,[c] Sifan Li,[a] Zhongling Lang,[b]* and Jiansheng Li[a,c]*

[a] School of Chemistry and Chemical Engineering, Liaoning Normal University, 116029, Dalian, Liaoning (China). *E-mail: sangxj923@lnnu.edu.cn, lijiansheng@lnnu.edu.cn*

[b] Key Laboratory of Polyoxometalate and Reticular Material Chemistry of Ministry of Education, Northeast Normal University, Changchun, 130024, Jilin (China). *E-mail: langzl554@nenu.edu.cn.*

[c] State Key Laboratory of Catalysis, iChEM, Dalian Institute of Chemical Physics, Chinese Academy of Sciences, Dalian National Laboratory for Clean Energy Dalian 116023, Liaoning (China). *E-mail: lijiansheng@dicp.ac.cn*

Experimental Section

Chemicals and Methods

All reagents are purchased commercially and used without further purification. $Na_2WO_4 \cdot 2H_2O$, H_3BO_3, HCl, DMF, KCl, KI, K_2CO_3, anhydrous piperazine, canuric chloride, 1,4−dioxane, potassium hydrogen phthalate ($C_8H_5KO_4$), Na_2SO_4, and other reagents are purchased commercially and used without further purification.

FTIR spectra were recorded on a Bruker AXS TENSOR−27 FTIR spectrometer in the range of 4000–400 cm^{-1}. Thermogravimetric (TG) analysis was performed on a Pyris Diamond TG-DTA (N_2 atmosphere) thermal analyzer at a heating rate of 10 °C min^{-1}. Ultraviolet-visible absorption spectra (UV-vis) were recorded using a Lambda 35 spectrometer. X-ray power diffraction (PXRD) data were collected on a Bruker AXS D8 Advance diffractometer using Cu Kα radiation (λ = 1.5418 Å). X-ray photoelectron spectroscopy (XPS) analysis was conducted on a VG ESCALAB MKII spectrometer using an Mg Kα (1253.6 eV) achromatic X-ray source. Scanning electron microscopy (SEM) was carried out on a JEOL ZXM6360−LV. The morphology of the nanostructured materials was characterized using an FEI Tecnai G2 F20 transmission electron microscope (TEM).

Synthesis of PC

PC was prepared according to the method reported in the literature. The specific steps were as follows: anhydrous piperazine (1.034 g, 12 mmol), K_2CO_3 (3.317 g, 24 mmol), and canuric chloride (1.476 g, 6 mmol) were added to a 250 mL flask containing 100 mL of 1,4−dioxane. The mixture was well stirred and placed in an oil bath under reflux at 110 °C for 48 hours. The solid product was obtained through extraction and filtration, followed by washing with dichloromethane, water, and ethanol three times. Finally, the solid product was dried overnight at 60 °C in an oven and PC was gained.[S1]

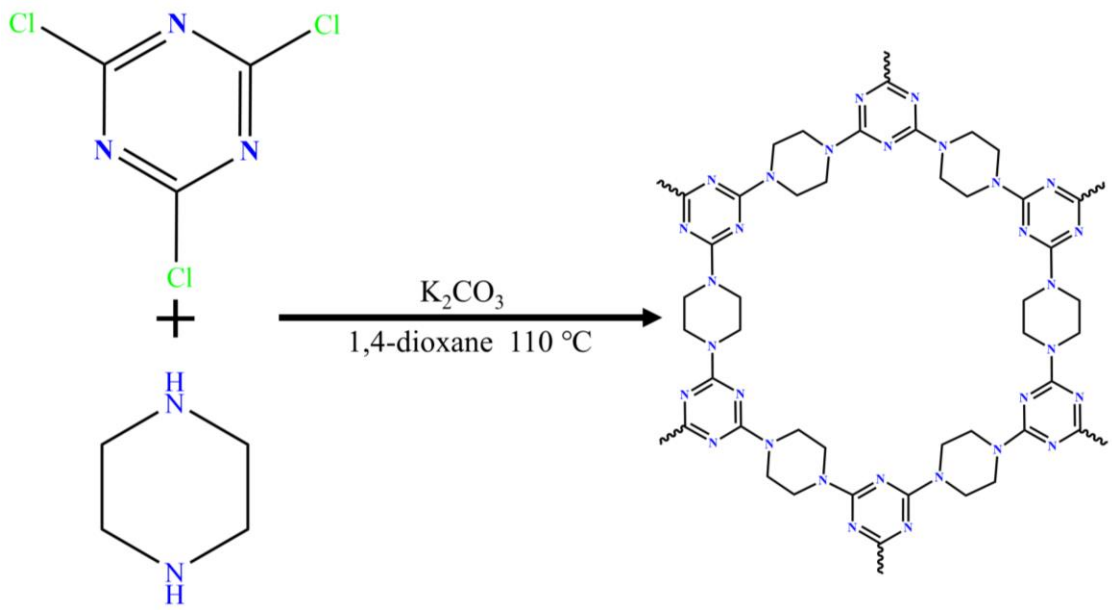

Scheme S1 The preparation process of PC.

Synthesis of $K_5[\alpha-BW_{12}O_{40}]\cdot xH_2O$

$K_5[\alpha-BW_{12}O_{40}]\cdot xH_2O$ was synthesized according to the method reported in the literature. The specific steps are as follows: $Na_2WO_4\cdot 2H_2O$ (20.0 g, 68 mmol) and H_3BO_3 (1.0 g, 16 mmol) were dissolved in 20 mL of deionized water successively, to which aqueous 6 M HCl was added under vigorous stirring until the pH of the mixture was adjusted to 6.0. After boiling for three hours, the pH of the reaction solution was adjusted to 2.0 with aqueous 6 M HCl. And then, the mixture was boiled for another 30 min. Finally, 2.0 g KCl was added to the solution, and colorless crystals were precipitated after 24 hours. The formula was denoted as BW_{12}.[S2]

Preparation of POMs@PC-X

0.2 g of PC was dispersed in 30 mL deionized water, to which an equal amount of BW_{12} was added and heated at 80 °C for 24 hours under stirring. The resulting solid was separated by centrifugation, followed by washing with water and ethanol three times, and dried overnight at 60 °C. Finally, the obtained powder was annealed in N_2 at different temperatures (200 °C, 250 °C and 300 °C) for 120 minutes in a tubular furnace with a heating rate of 5 °C min^{-1}, and the as-prepared composite materials

were denoted as BW_{12}@PC-200, BW_{12}@PC-250 and BW_{12}@PC-300, respectively. Meanwhile, BW_{12}@PC-250-Air was prepared with the same procedure of BW_{12}@PC-250 except that N_2 was replaced by air during annealing. In addition, various composite materials denoted as xBW_{12}@PC-250 (x represents the mass ratios between BW_{12} and PC, x = 0.5, 1.0, 2.0, 3.0, and 5.0, in which 1.0BW_{12}@PC-250 was denoted as BW_{12}@PC-250) as well as PW_{12}@PC-250 and SiW_{12}@PC-250 were also prepared for comparison with the similar method.

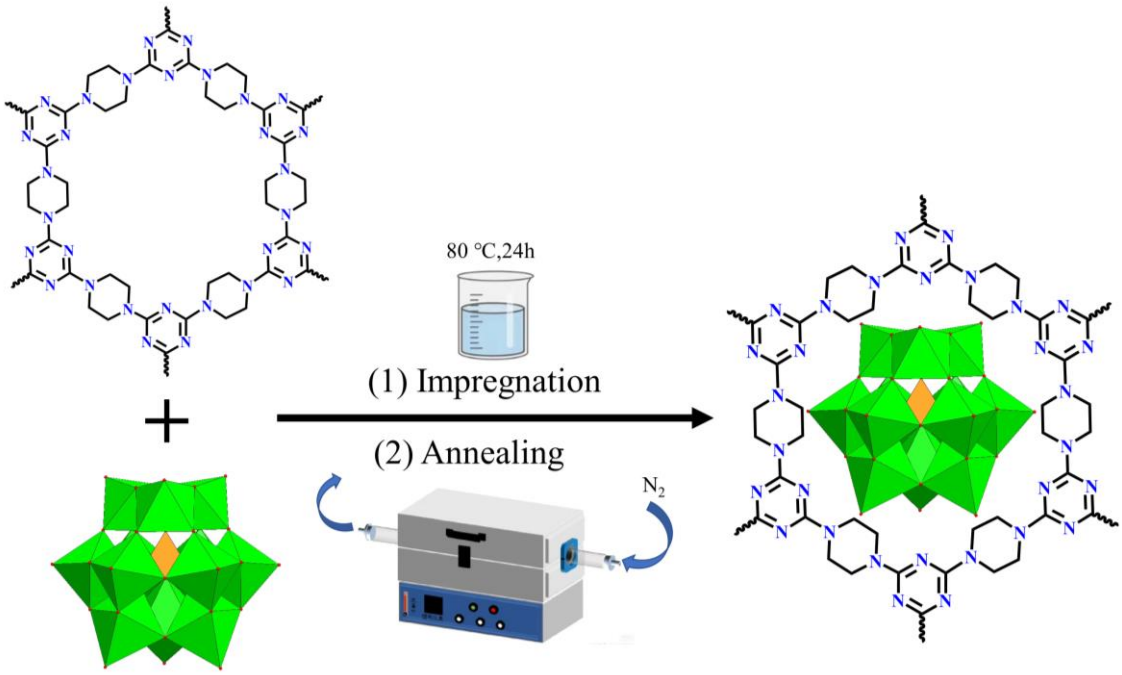

Scheme S2 The schematic preparation process of POMs@PC-X (X represents the annealing temperature in N_2).

Photocatalytic performance

The photocatalytic procedures were conducted in a quartz reactor placed in an ice-water bath to keep the reaction system at about 10 °C. Specifically, 50 mg of photocatalysts were dispersed in 100 mL distilled water by ultrasonic treatment for five minutes. After dark reaction for 30 min, the photocatalytic reaction was triggered by using the Xe lamp as light source (CEAULIGHT, CEL−HXF300T3, CEL−HXUV300T3, λ>320 nm). O_2 was bubbled continuously during the whole process. The concentration of produced H_2O_2 was measured every 30 min by iodometry. The specific process was as follows: 1.0 mL of 0.1 M potassium hydrogen phthalate

($C_8H_5KO_4$) aqueous solution was mixed with 1.0 mL 0.4 M potassium iodide (KI) aqueous solution, and then 1.0 mL of the reaction supernatant was added. After reaction under dark for 30 min, the absorbance at 350 nm was measured by recording the UV-vis absorption spectra. The Schematic diagram of photocatalytic experiment is shown in Scheme S3 and the standard curve of H_2O_2 concentration measured by iodimetry is shown in Fig. S1.

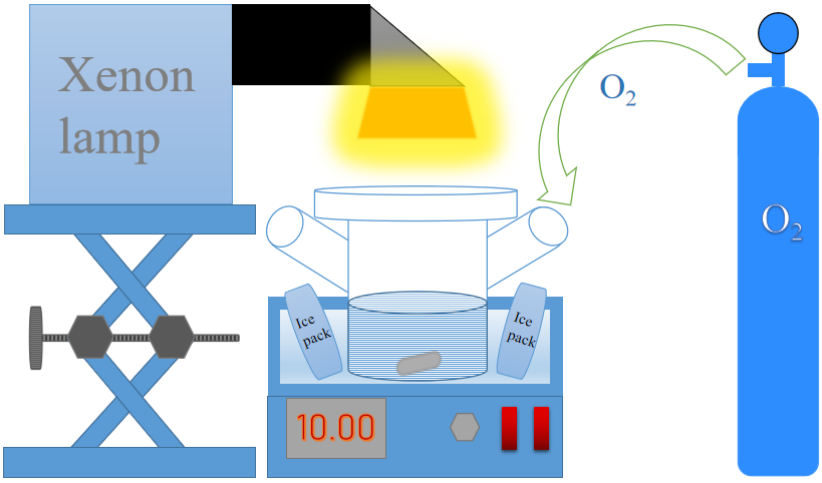

Scheme S3 Schematic diagram of photocatalytic experiment.

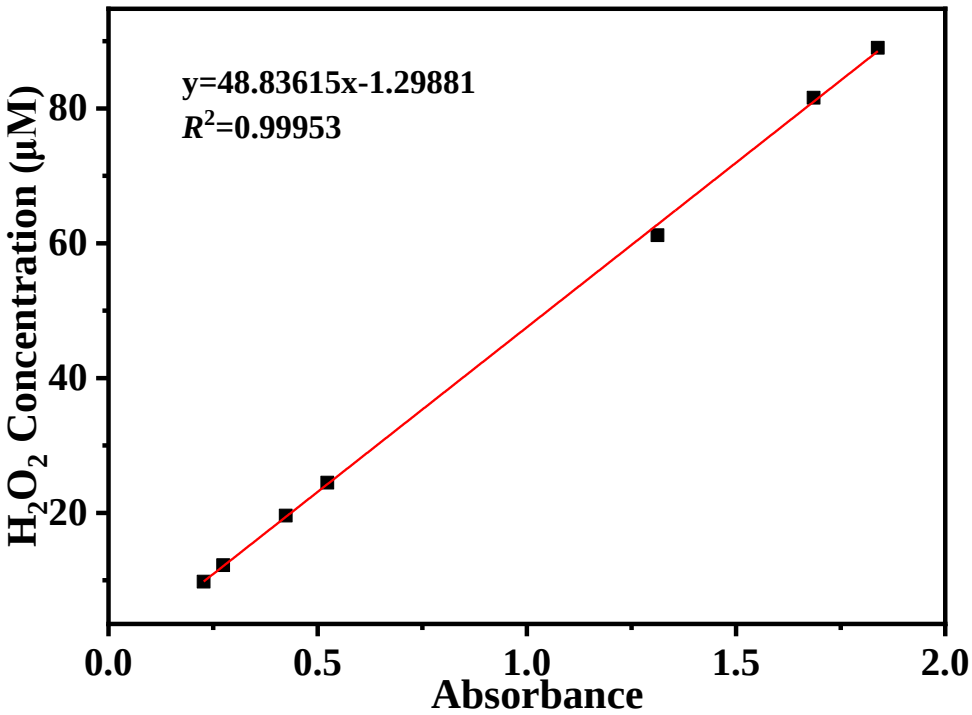

Fig. S1 Standard curve for detecting H_2O_2 concentration by iodimetry.

Photoelectrochemical measurements

Transient photocurrent response, linear sweep voltammetry (LSV), Mott−Schottky plot and electrochemical impedance spectroscopy (EIS) were conducted in 0.5 M Na_2SO_4 solution by a three-electrode system which comprises photocatalyst-loaded FTO as working electrode, platinum wire as counter electrode, and Ag/AgCl as reference electrode. The working electrode was prepared as follows: 5 mg of photocatalyst and 100 μL of Nafion solution (5%) were blended into 900 μL of DMF to form the stock solution. Subsequently, 10 μL of the stock solution was drop-coated on a clean FTO with an area of 1 cm^2. After drying under ambient condition, the working electrode was obtained.[S3]

DFT calculations

All optimization and property calculations were performed within the generalized gradient approximation (GGA) and Perdew–Burke–Ernzerhof (PBE) functional as implemented in the VASP code.[S4, S5] The electron−ion interaction is described using the projector−augmented plane wave (PAW) scheme.[S6, S7] The kinetic energy cut off was set to 400 eV. All the atoms in the cell were allowed to relax during the geometric optimizations until the energy convergence threshold and forces were smaller than 10^{-5} eV and 0.03 eV $Å^{-1}$. Reciprocal space was described by using the Monkhorst–Pack algorithm under 3 × 3 × 1 sampling.[S8] Finally, all the optimized structures were characterized as suitable minima. The post−processing of energy corrections (zero−point energy and entropy) was performed with the help of the VASPKIT code.[S9] The charge transfers between PC and BW_{12} were conducted by the Bader charge analysis.[S10] The formation energy (E_{form}) is defined as the relations of Eform = EPOM@PC – EPOM – EPC, where EPOM@PC, EPOM, EPC are the energy of BW_{12}@PC, BW_{12}, PC. The Gibbs free energy changes ΔG along ORR pathways was analyzed by the computational hydrogen electrode (CHE) model put forward by Nørskov et al.[S11]

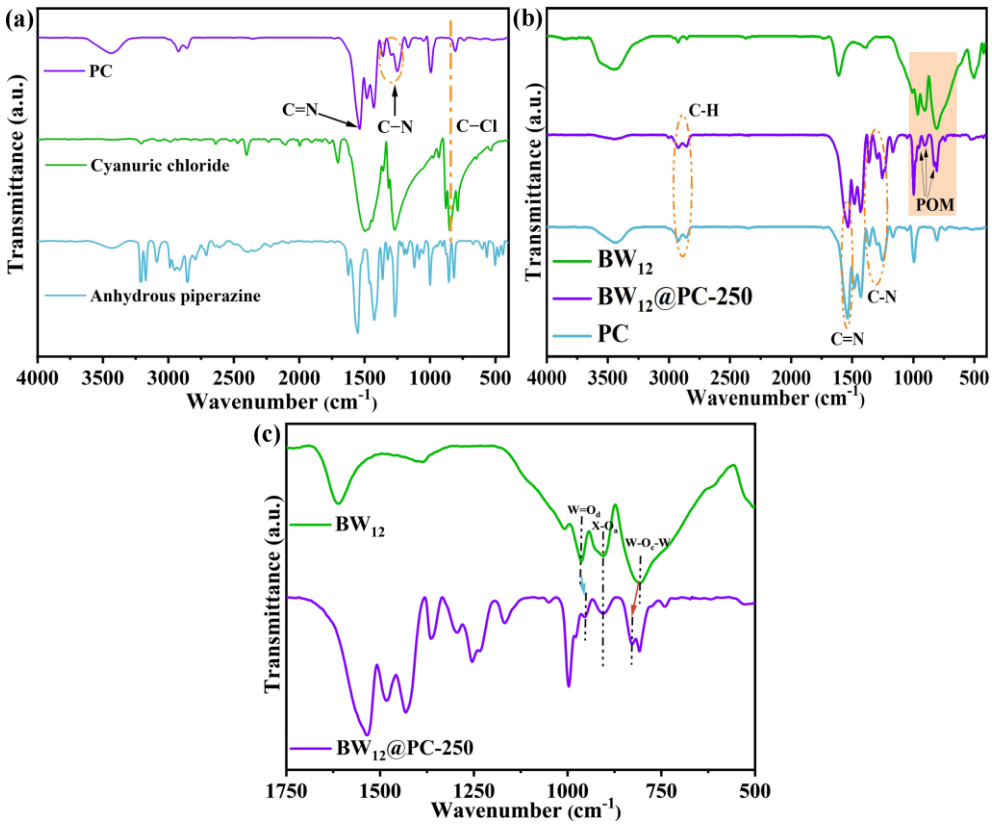

Fig. S2 FTIR spectra of (a) PC (purple), cyanuric chloride (green), anhydrous piperazine (blue); (b) BW_{12} (green), PC (blue), BW_{12}@PC-250 (purple); (c) the enlarged area of the orange rectangle in Fig. S2b.

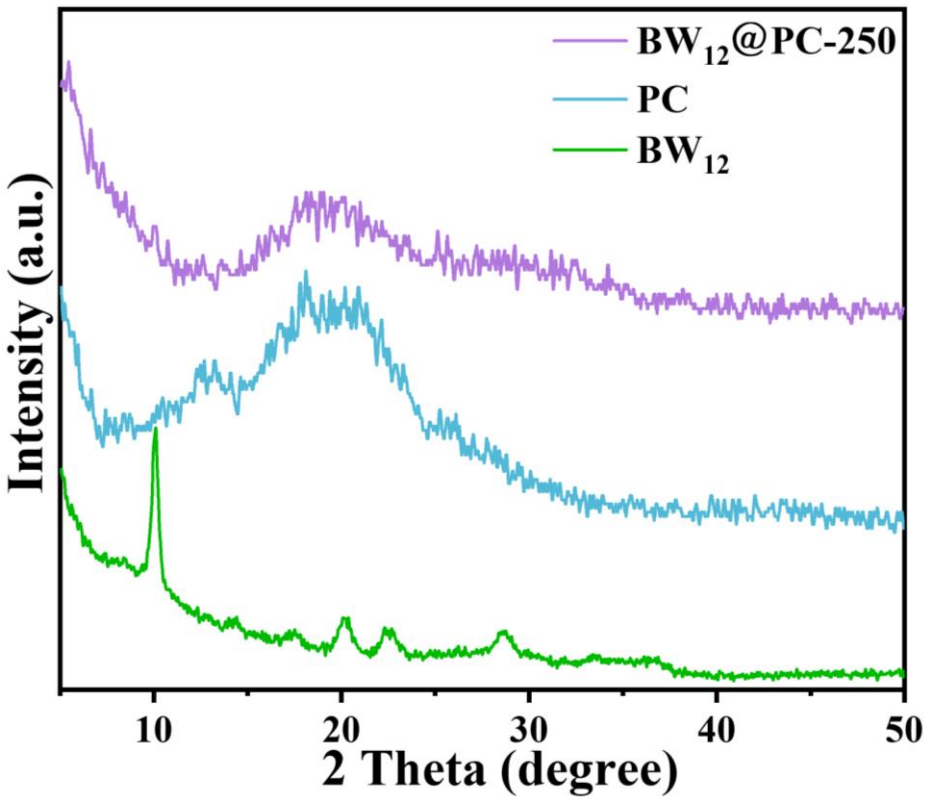

Fig. S3 PXRD patterns of BW_{12} (green), PC (blue) and BW_{12}@PC-250 (purple).

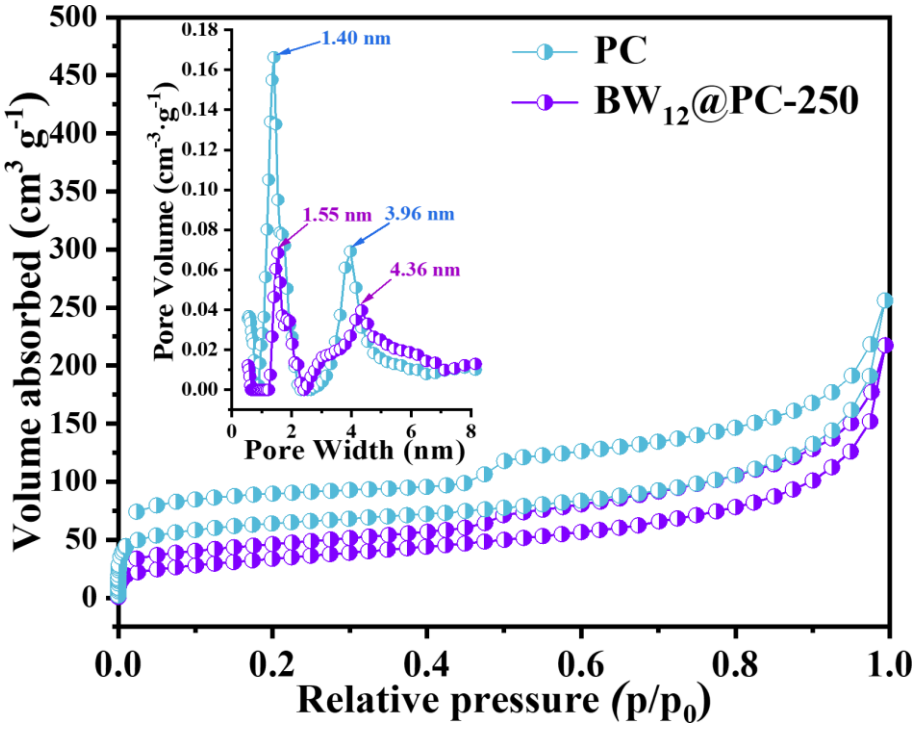

Fig. S4 Nitrogen adsorption-desorption isotherms and pore size distribution curves (inset) of PC (blue) and BW_{12}@PC-250 (purple)

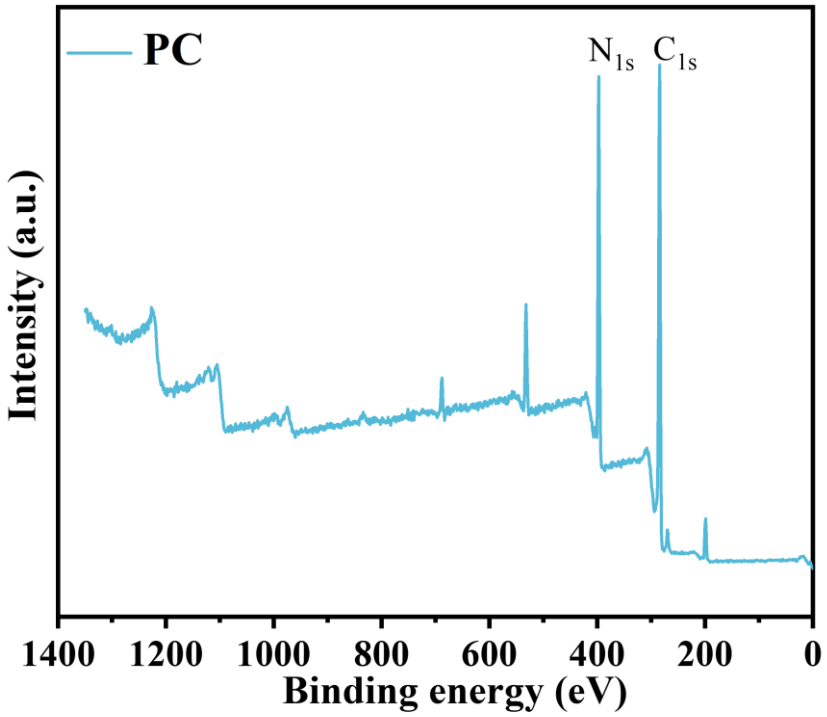

Fig. S5 XPS survey spectrum of PC.

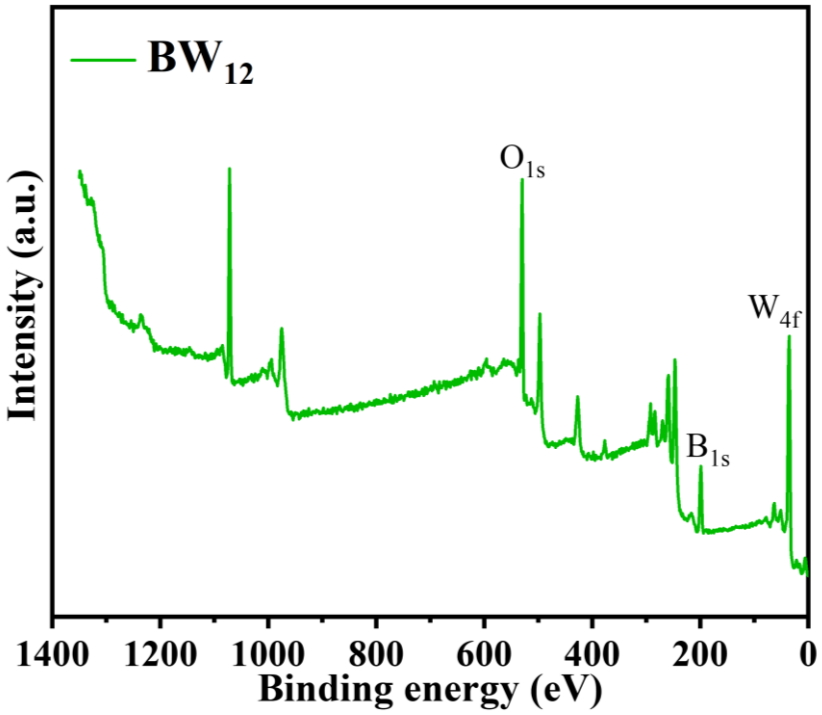

Fig. S6 XPS survey spectrum of BW_{12}.

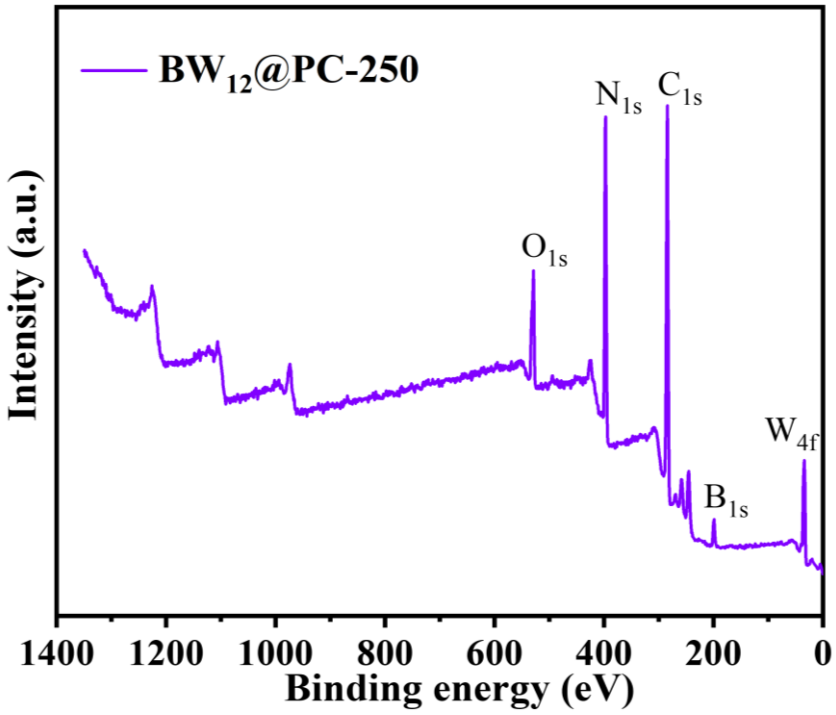

Fig. S7 XPS survey spectrum of BW_{12}@PC-250.

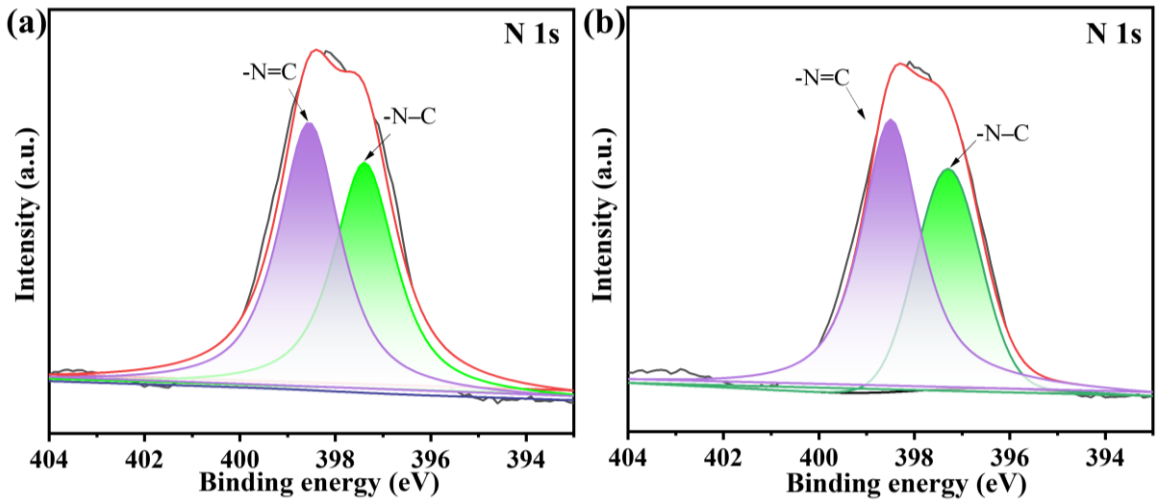

Fig. S8 N 1s XPS spectra of BW_{12}@PC-250 (a) and PC (b).

Fig. S8 shows the N 1s peak, which can be further divided into N=C (398.5 eV) and N−C (397.4 eV) (Fig. S8a, b), corresponding to the nitrogen species in triazine and piperazine, respectively.[S12]

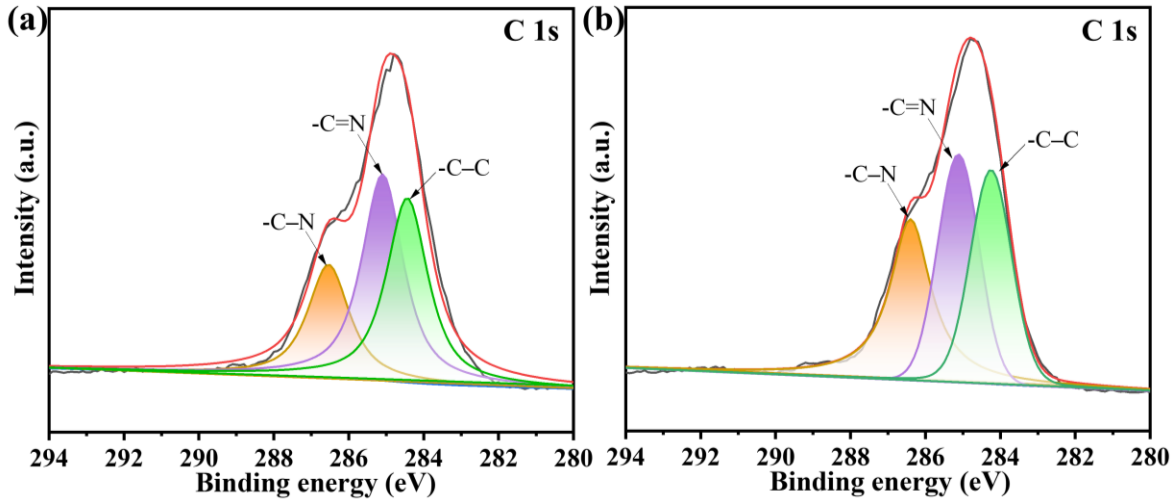

Fig. S9 C 1s XPS spectra of BW_{12}@PC-250 (a) and PC (b).

Fig. S9 shows the C 1s spectrum is divided into three fitting peaks (Fig. S9a, b), namely, C−C (284.4 eV), C=N (285.1 eV), and C−N (286.5 eV), confirming the successful synthesis of PC. [S12]

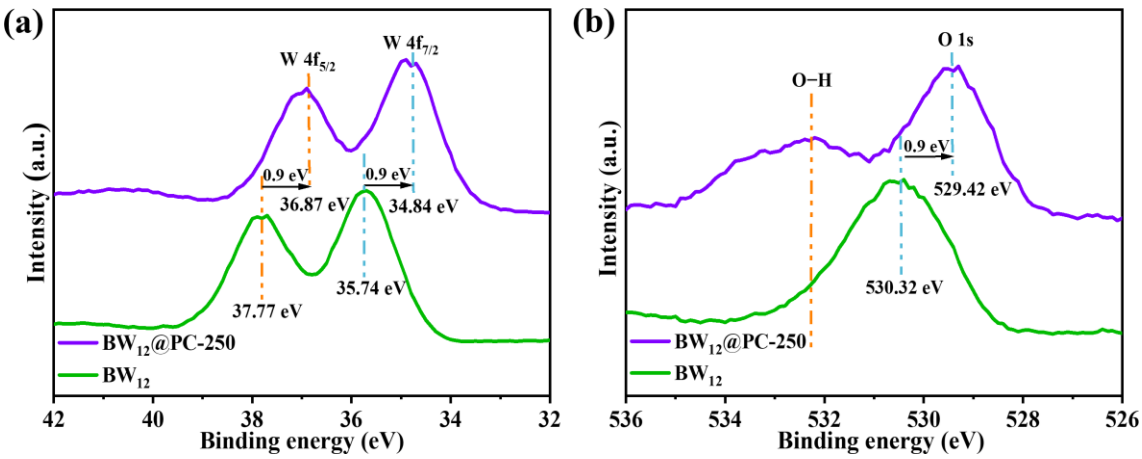

Fig. S10 W 4f XPS spectra of BW_{12}@PC-250 (a) and BW_{12} (b).

For W 4f XPS spectrum, the peaks at 36.87 eV and 34.84 eV are separately assigned to W(VI) $4f_{5/2}$ and W(VI) $4f_{7/2}$ in BW_{12}@PC-250, while the peaks at 37.77 eV and 35.74 eV are separately attributed to W(VI) $4f_{5/2}$ and W(VI) $4f_{7/2}$ in BW_{12} (Fig. S10a).

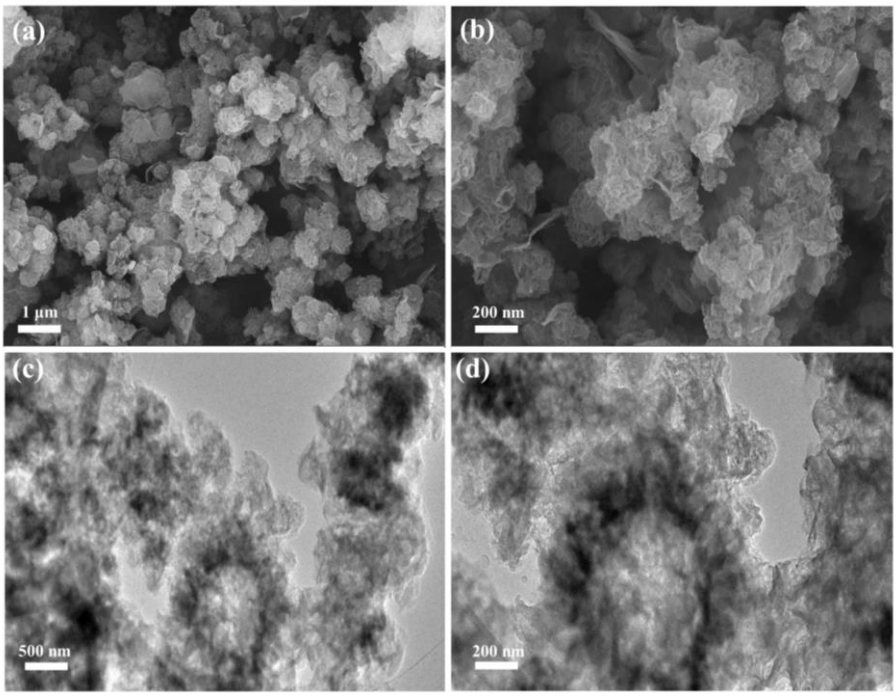

Fig. S11 SEM images of PC (a, b) and TEM images of PC (c, d).

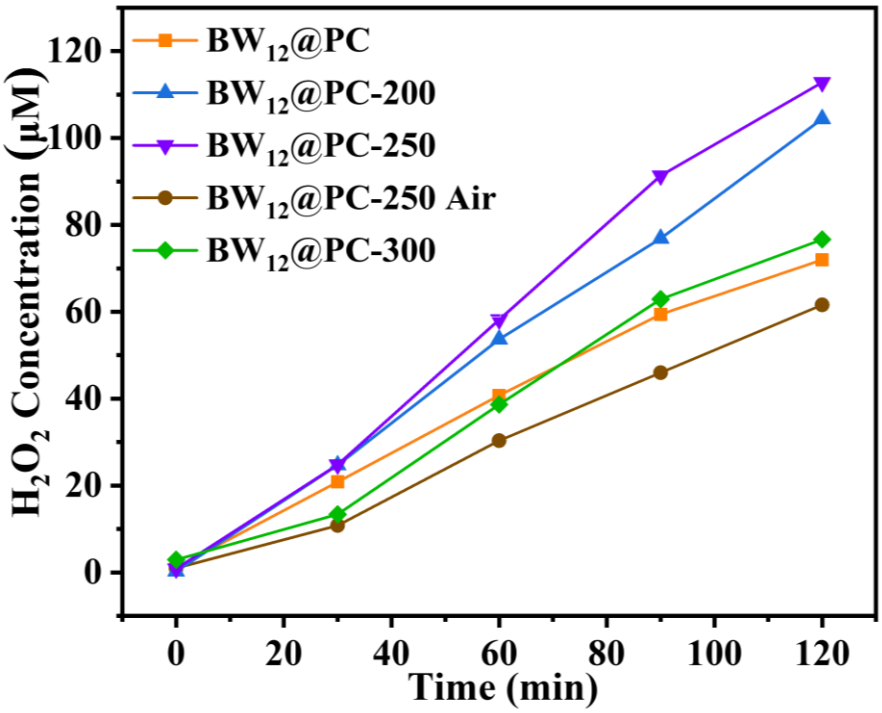

Fig. S12 Production of H_2O_2 with BW_{12}@PC, BW_{12}@PC-X (X represents the annealing temperature of BW_{12}@PC in N_2, X = 200, 250 and 300), and BW_{12}@PC-250-Air that was prepared by annealing of BW_{12}@PC at 250 °C in air as photocatalysts, respectively in pure water using 300 W Xe lamp as light source.

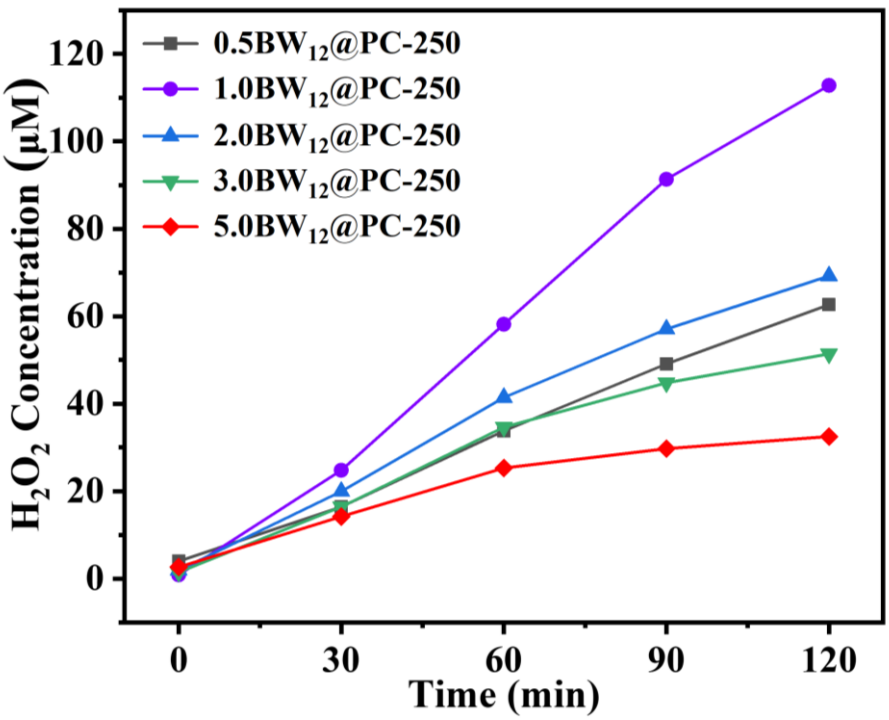

Fig. S13 Production of H_2O_2 with xBW_{12}@PC-250 (x represents the mass ratio of BW_{12} and PC during preparation of composite materials, x = 0.5, 1.0, 2.0, 3.0 and 5.0, in which 1.0BW_{12}@PC-250 was denoted as BW_{12}@PC-250) as photocatalysts in pure water using 300 W Xe lamp as light source.

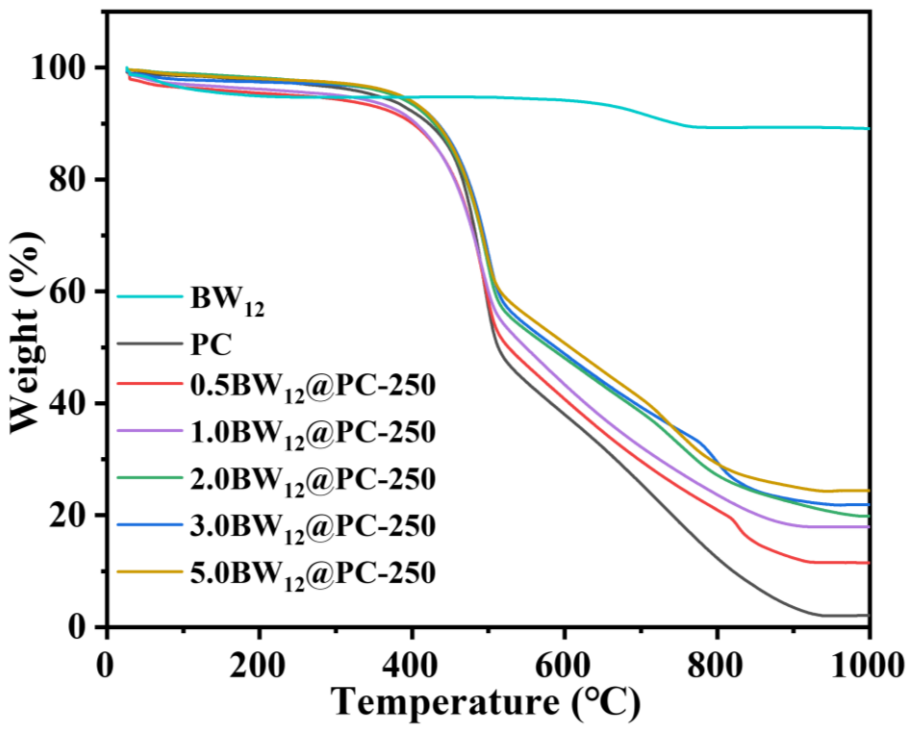

Fig. S14 TGA curves of PC and xBW_{12}@PC-250 (x = 0.5, 1.0, 2.0, 3.0 and 5.0).

By adjusting the mass ratio (x) of BW_{12} and PC during preparation of composite materials, the photocatalytic performance of xBW_{12}@PC−250 (x represents the mass ratios between BW_{12} and PC, x = 0.5, 1.0, 2.0, 3.0 and 5.0) with different loading of BW_{12} was investigated (Fig. S13). The loading of BW_{12} in xBW_{12}@PC−250 was evaluated through the thermogravimetric analysis (TGA) curves (Fig. S14), from which it is concluded that the loading of BW_{12} is increasing gradually with the increase of mass ratio. The content of BW_{12} was calculated by TGA as show in Table S1.[S13]

Table S1 The loading of BW_{12} in xBW_{12}@PC-250 (x presents the mass ratio of BW_{12} and PC during impregnation process)

Sample	wt% of BW_{12}
$0.5BW_{12}$@PC-250	3.71%
$1.0BW_{12}$@PC-250	10.14%
$2.0BW_{12}$@PC-250	12.06%
$3.0BW_{12}$@PC-250	14.11%
$5.0BW_{12}$@PC-250	16.61%

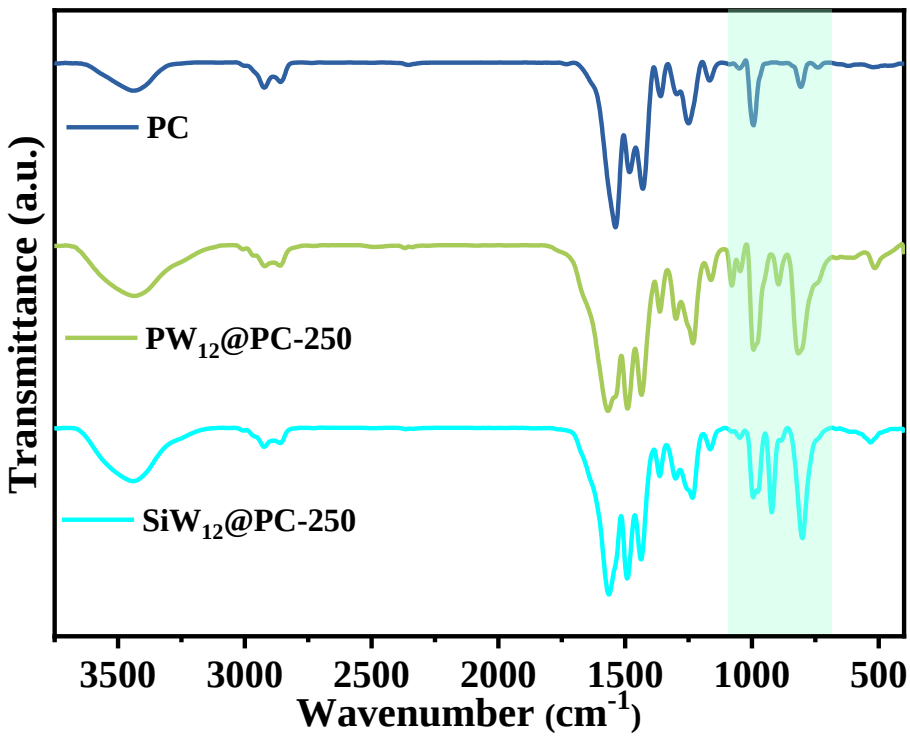

Fig. S15 FTIR spectra of PC and POM@PC-250 (POM = PW_{12}, SiW_{12}).

Fig. S15 illustrates the FTIR spectra of PC, PW_{12}@PC-250 and SiW_{12}@PC-250, from which it can be seen that the characteristic peaks of PC remain almost unchanged in the FTIR spectra of both PW_{12}@PC-250 and SiW_{12}@PC-250, proving that the structure of PC keeps intact after incorporation of PW_{12} and SiW_{12}. In addition, the characteristic peaks of PW_{12} and SiW_{12} are observed in PW_{12}@PC-250 and SiW_{12}@PC-250, indicating the successful embedding of PW_{12} and SiW_{12}.[S2]

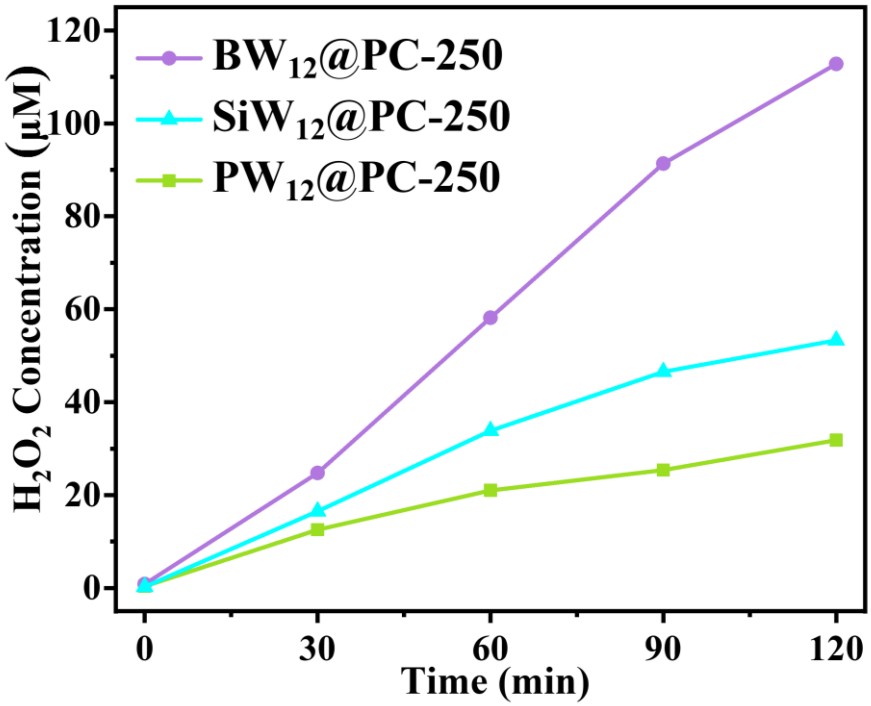

Fig. S16 Production of H_2O_2 with different POMs@PC-250 (POM = BW_{12}, SiW_{12} and PW_{12}).

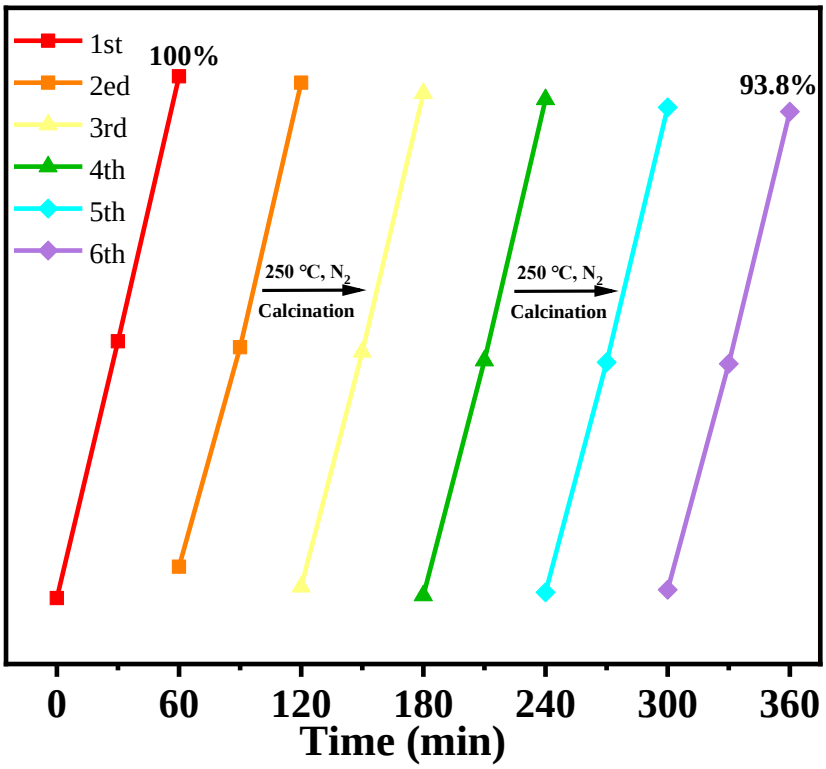

Fig. S17 Recycle performance of BW_{12}@PC-250.

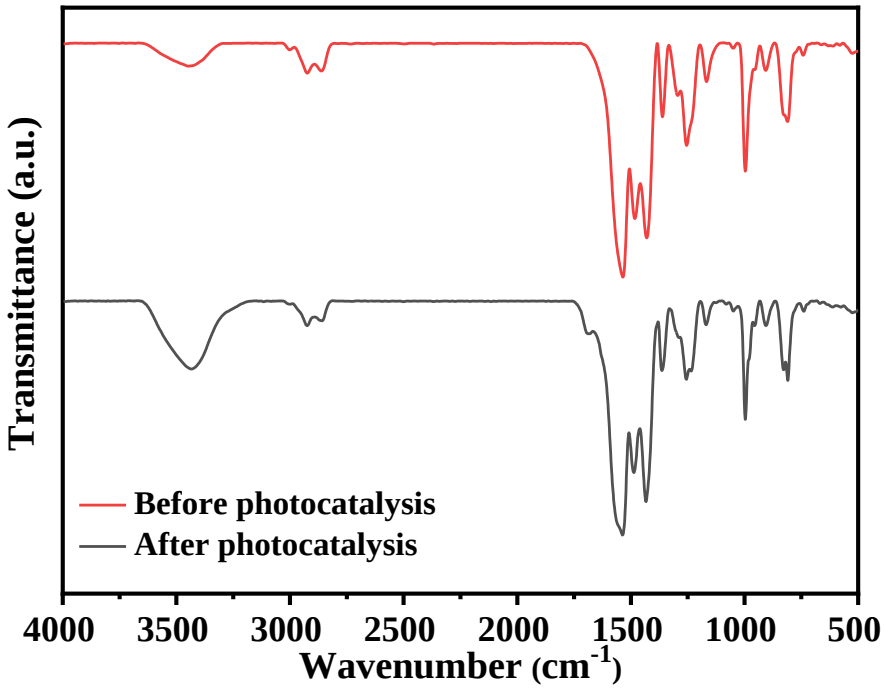

Fig. S18 FTIR spectra of BW_{12}@PC-250 before and after photocatalysis

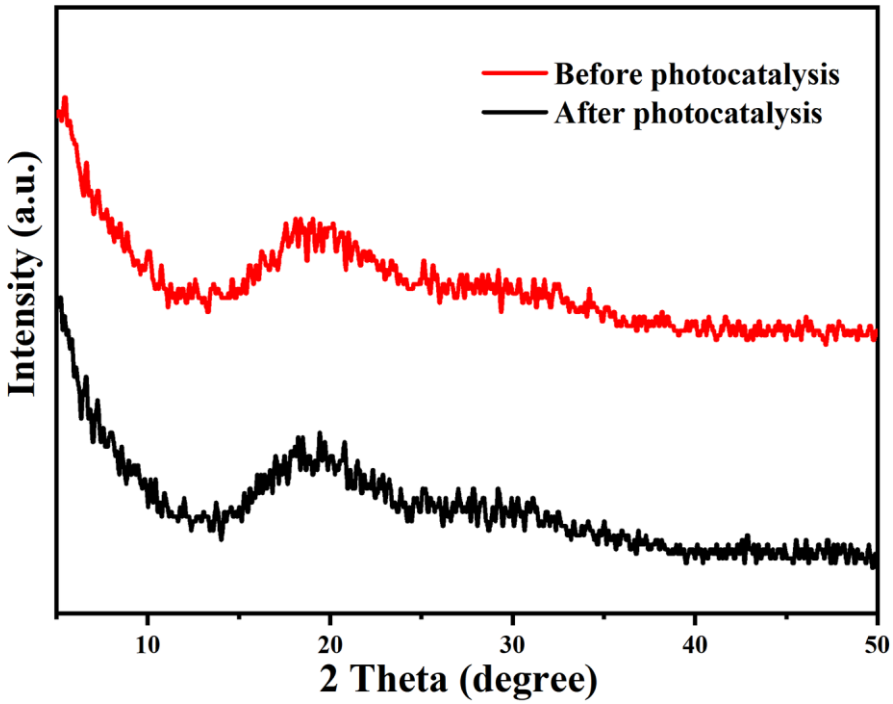

Fig. S19 PXRD patterns of BW_{12}@PC-250 before and after photocatalysis.

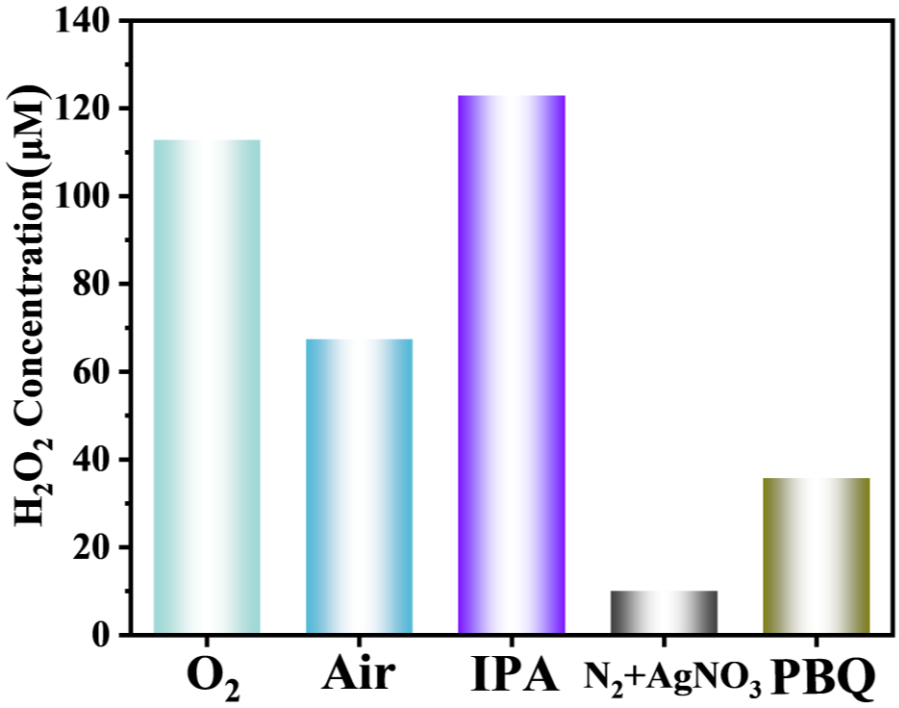

Fig. S20 Effects of different atmospheres and different sacrificial agents on H_2O_2 yield.

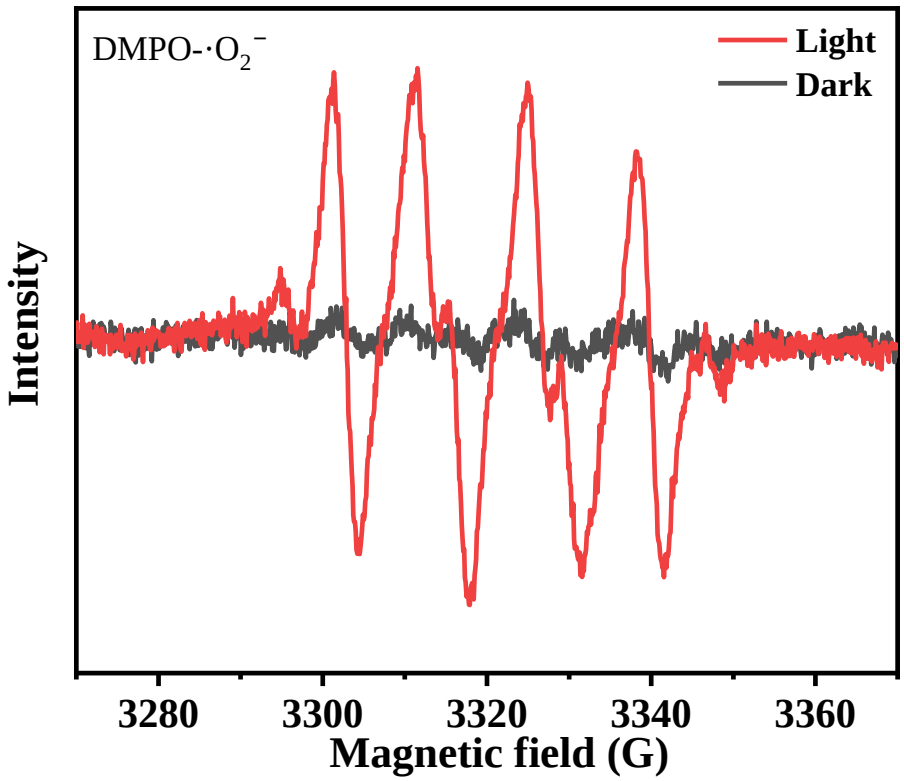

Fig. S21 EPR spectra of BW_{12}@PC-250 under dark and light conditions using DMPO as a spin-trap agent.

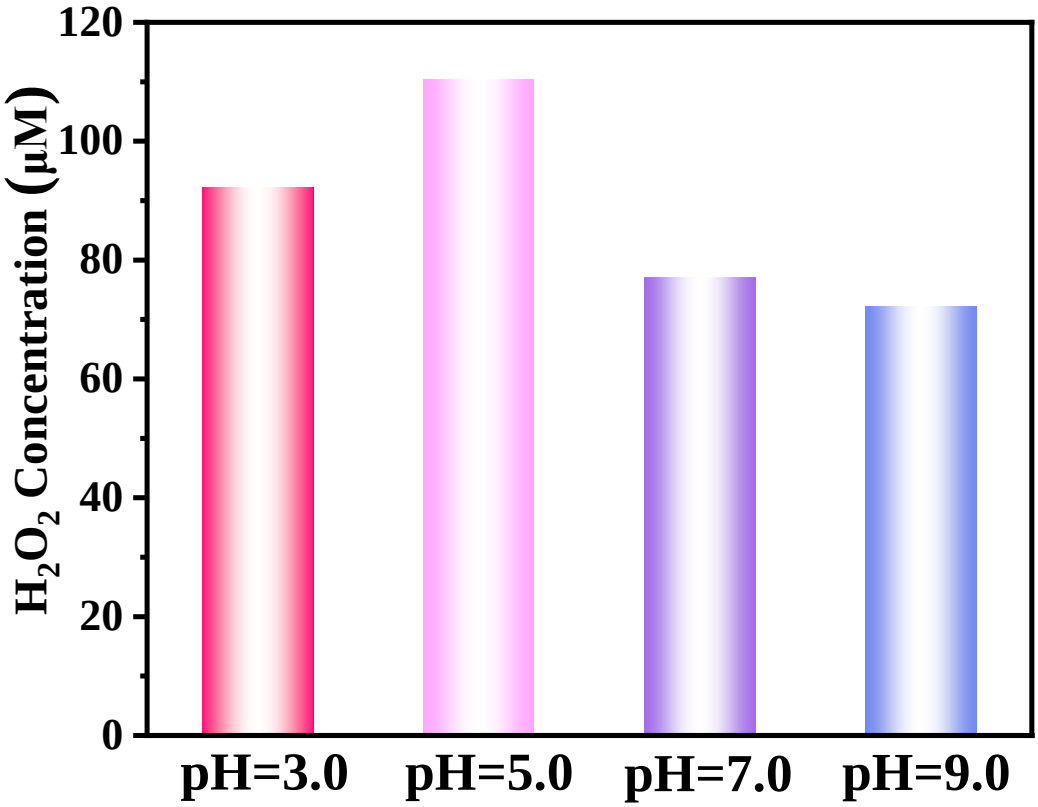

Fig. S22 Effect of initial pH on H_2O_2 yield.

The effect of initial pH on the photosynthesis of H_2O_2 is studied by adjusting the pH of photocatalytic solution with 0.1 M HCl or KOH solution.

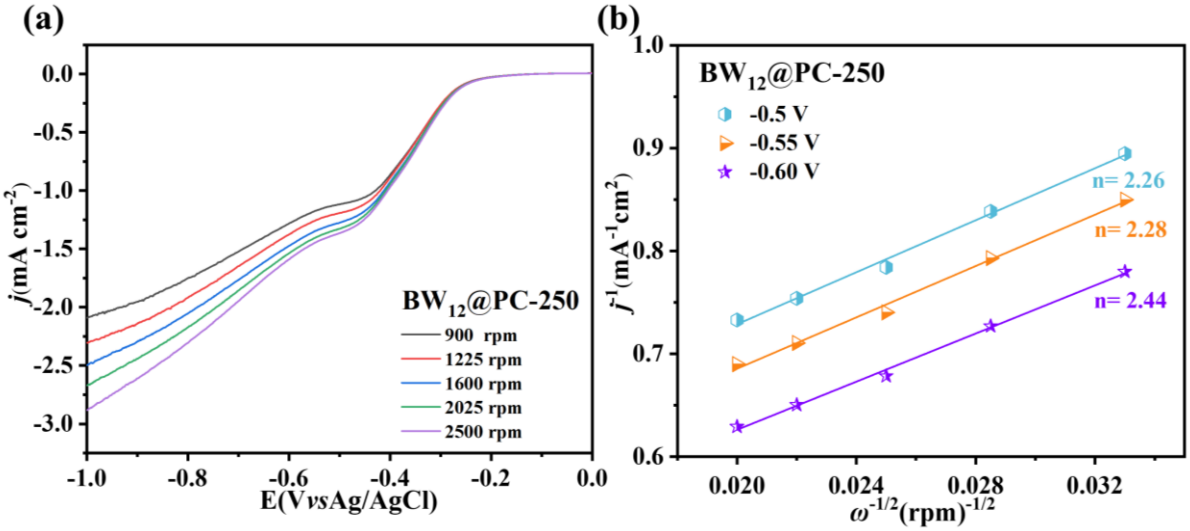

Fig. S23 (a) LSV curves of BW_{12}@PC-250 by RDE and (b) calculation of the average electron transfer numbers through LSV curves.

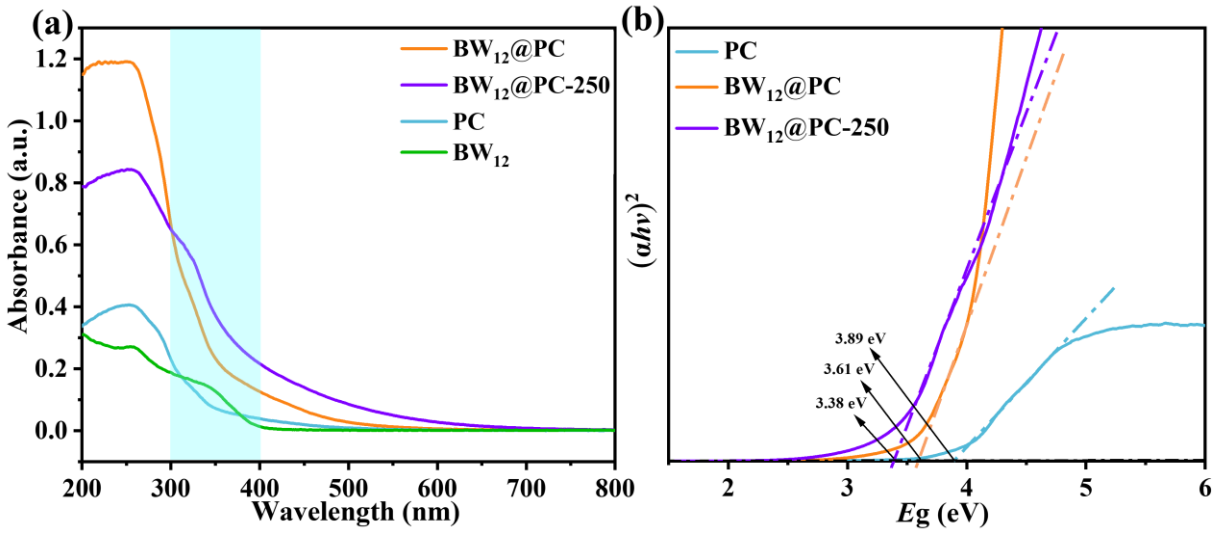

Fig. S24 (a) Solid state UV−vis diffuse reflection absorption spectra and (b) Tauc plots of different catalysts.

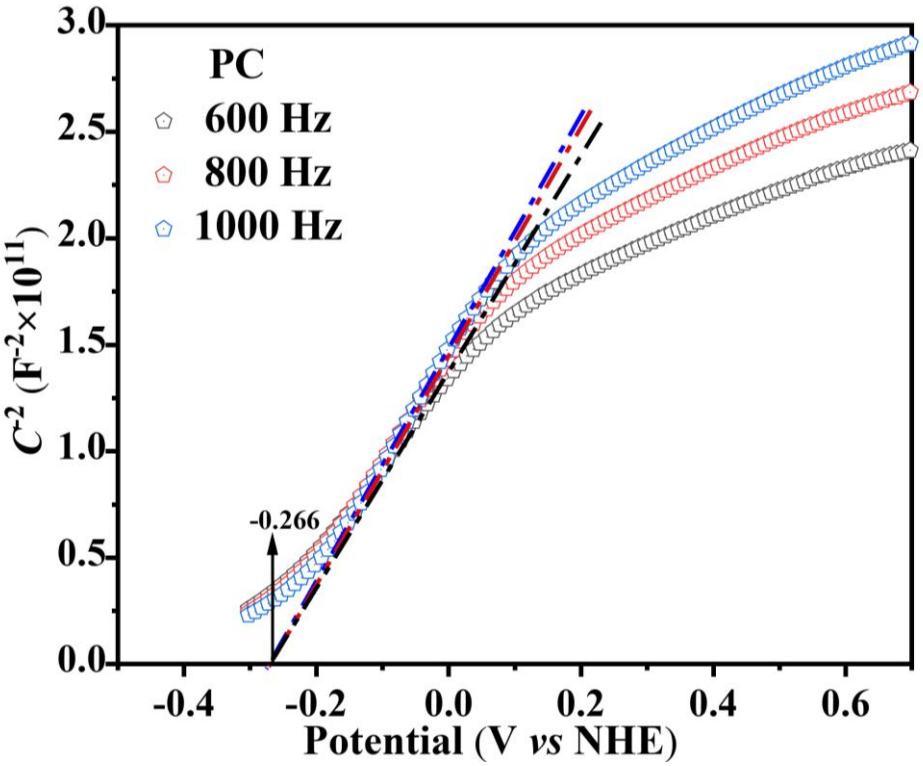

Fig. S25 Mott-Schottky plot of PC.

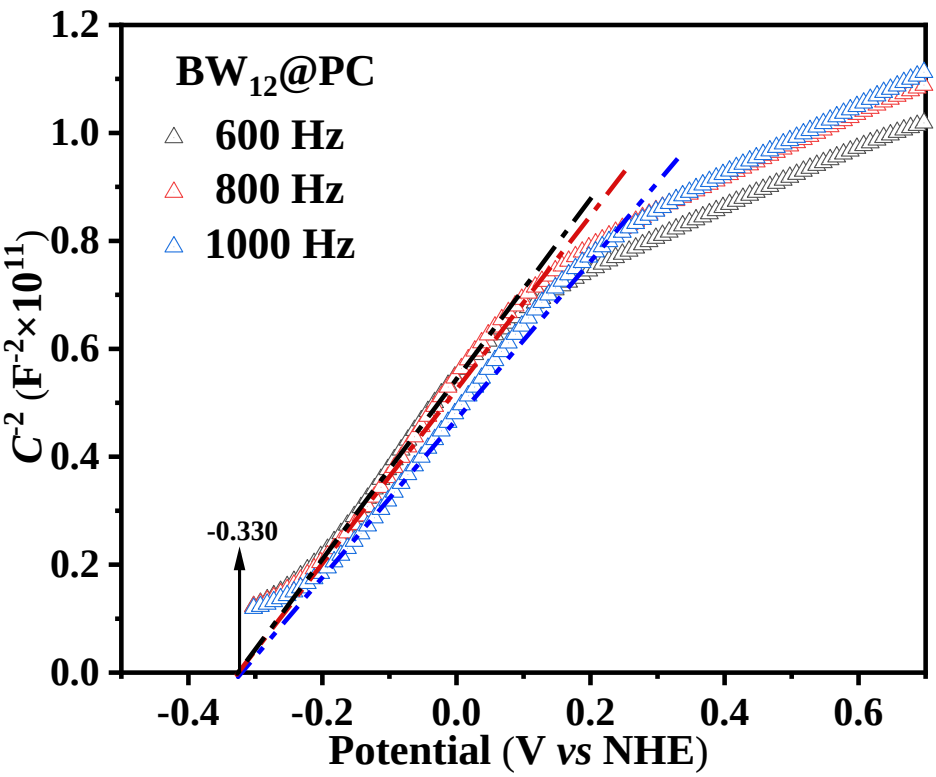

Fig. S26 Mott-Schottky plot of BW_{12}@PC.

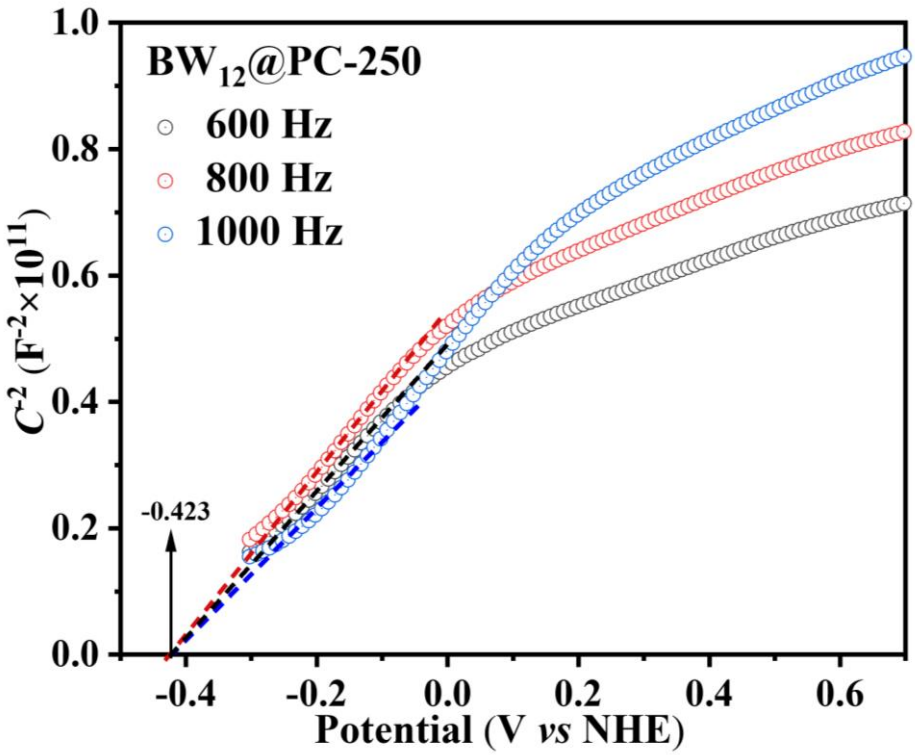

Fig. S27 Mott-Schottky plot of BW_{12}@PC-250.

The Mott-Schottky (M-S) plots (Figs. S25−S27) of BW_{12}@PC-250, BW_{12}@PC and PC were measured to obtain their flat band potential, which were −0.423, −0.330 and

−0.266 V vs. NHE, respectively. Accordingly, the positions of conduction bands (CBs) of BW_{12}@PC-250, BW_{12}@PC and PC were estimated to be −0.523, −0.430 and −0.366 V vs. NHE in consideration of the fact that the energy level of CB is usually 0−0.1 V more negative than the flat band potential.

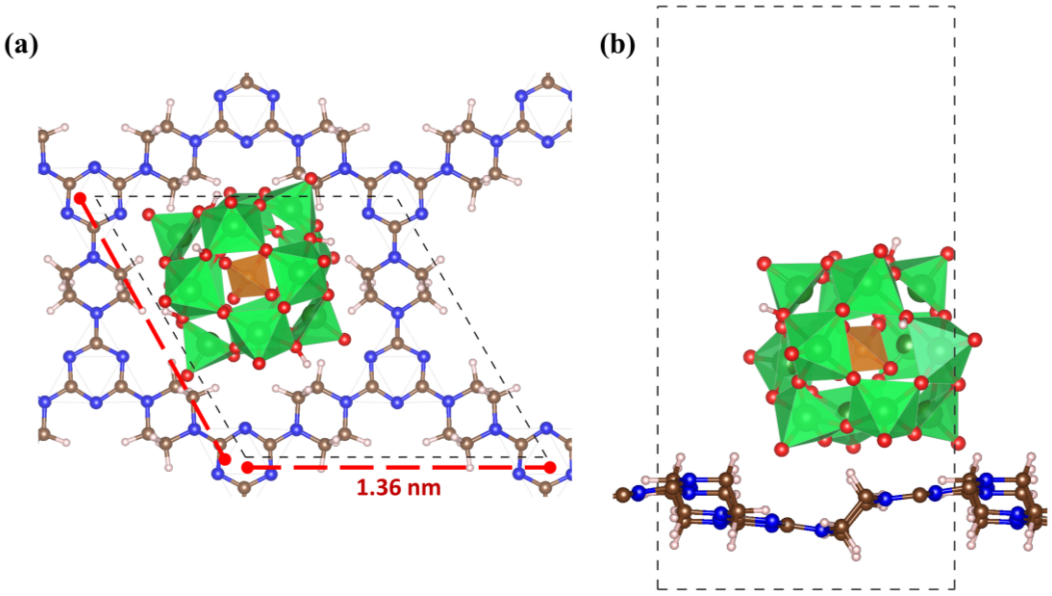

Fig. S28 The top and side views of BW_{12}@PC.

The following DFT calculations were performed. The PC with C_3 point group was constructed, and a vacuum region of 30 Å was used to eliminate the interlayer interaction. The POM (BW_{12}) included five H as the counterbalance ion and combined with PC through hydrogen interaction, and a top and side views of BW_{12}@PC was illustrated in Fig. S28.

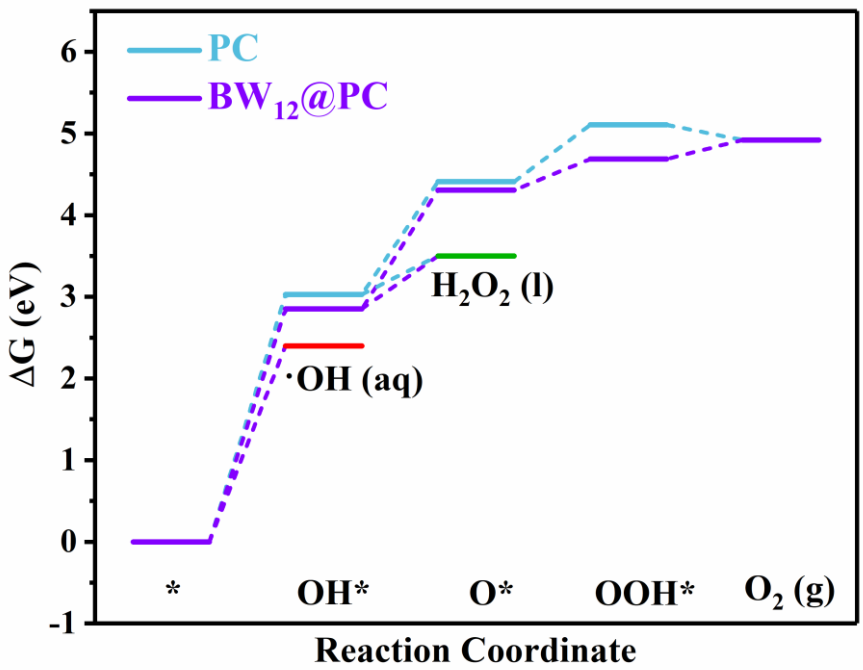

Fig. S29 Free energy diagrams of the one, two, and four electron processes for water oxidation of PC and BW_{12}@PC.

Calculations of the aqueous oxidation process show that the active site of the reaction occurs at the C atom of the triazine, and during water oxidation the weak adsorption of OH* leads to hydroxyl radicals being the main product, only a small amount of H_2O_2 may be produced by BW_{12}@PC.[S14] Therefore, H_2O_2 is produced mainly by the two step one electron reduction of O_2. H_2O is the electron and hydrogen donor for the ORR.

Reference

S1 X. Hu, Y. Long, M. Fan, M. Yuan, H. Zhao, J. Ma and Z. Dong, *Appl. Catal. B*, 2019, **244**, 25-35.

S2 C. Rocchiccioli-Deltcheff, M. Fournier, R. Franck and R. Thouvenot, *Inorg. Chem*, 1983, **22**, 207-216.

S3 S. Zhou, H. Hu, H. Hu, Q. Jiang, H. Xie, C. Li, S. Gao, Y. Kong and Y. Hu, *Sci. China Mater.*, 2023, **66**, 1837-1846.

S4 G. Kresse and J. Furthmüller, *Comput. Mater. Sci.*, 1996, **6**, 15-50.

S5 G. Kresse and J. Furthmuller, *Phys. Rev., B Condens. Matter*, 1996, **54**, 11169-11186.

S6 P. E. Blochl, *Phys. Rev., B Condens. Matter*, 1994, **50**, 17953-17979.

S7 J. Paier, M. Marsman, K. Hummer, G. Kresse, I. C. Gerber and J. G. Angyan, *J. Chem. Phys.*, 2006, **124**, 154709.

S8 H. J. Monkhorst and J. D. Pack, *Phys. Rev. B*, 1976, **13**, 5188-5192.

S9 V. Wang, N. Xu, J.-C. Liu, G. Tang and W.-T. Geng, *Comput Phys Commun*, 2021, **267,**

108033.
S10 G. Henkelman, A. Arnaldsson and H. Jónsson, *Comput. Mater. Sci.*, 2006, **36**, 354-360.
S11 J. K. Nørskov, J. Rossmeisl, A. Logadottir, L. Lindqvist, J. R. Kitchin, T. Bligaard and H. Jónsson, *J. Phys. Chem. B*, 2004, **108**, 17886-17892.
S12 X. Shen, J. Zhang, H. Jiang, Y. Du and R. Chen, *Ind. Eng. Chem. Res*., 2022, **61**, 4534-4545.
S13 S. Zhao, X. Zhao, S. Ouyang and Y. Zhu, *Catal. Sci. Technol.*, 2018, **8**, 1686-1695.
S14 S. Siahrostami, G. L. Li, V. Viswanathan, and J. K. Nørskov, *J. Phys. Chem. Lett.*, 2017, **8**, 1157-1160.